Raman scattering from $Ge_{1-x}Sn_x$ ($x \leq 0.14$) alloys

H. Navarro-Contreras, A.G. Rodríguez, and M.A. Vidal
Coordinación para la Innovación y la Aplicación de la Ciencia y la Tecnología, Universidad Autónoma de San Luís Potosí, Álvaro Obregón 64, San Luis Potosí, S.L.P. 78000, México.

H. Pérez-Ladrón de Guevara
Centro Universitario de los Lagos, Universidad de Guadalajara, Av. Enrique Díaz de León 1144, Col. Paseos de la Montaña, Lagos de Moreno, Jal. 47460, México.

Received 5 November 2014; accepted 18 August 2015

$Ge_{1-x}Sn_x$ alloys with x concentration up to 0.14 were grown on Ge(001) and GaAs(001) substrates in a conventional R. F. Magnetron Sputtering system at low substrate temperatures. The structural characteristics of these alloys were studied for different Sn concentrations between 1 to 14 % by high resolution X ray diffraction, and Raman spectroscopy. Contrasting characteristics of the grown layers are observed if the Sn concentration is larger or smaller than 6 % as revealed by X-ray diffraction and Raman spectroscopy.

Keywords: Raman; space correlation model.

PACS: 68; 68.35.bg

1. Introduction

$Ge_{1-x}Sn_x$ alloys, pertaining to the IV-IV column of the periodic table, have been a subject of interest for the last two decades, due to the very attractive possibility to fabricate with them materials consisting of elements of the column IV that may have a direct electronic band gap tunable from 0 to near 0.55 eV [1]. The study is driven by the interest to apply them as systems to produce far and medium infrared diodes, photodetectors [2,3] and lasers [4,5]; hence, as a very convenient substitute for the Hg-Cd-Te system [6]. These alloys have also been used as buffer layers for a complete integration between Ge or the ternary alloy $Ge_{1-x-y}Si_xSn_y$ on Si substrates, instead of $Si_{1-x}Ge_x$ alloys [7-9]. Calculations in the strong bonding models [10] and from pseudopotential methods [11] in the virtual crystal approximation, have predicted that $Ge_{1-x}Sn_x$ alloys must exhibit a direct band gap somewhere in the tin composition range between $x = 0.2$ to 0.5 eV in non-stressed films [12]. Additionally, due to the prevalence of covalent bonding of both Ge and Sn, and similar external electronic configurations, it has been predicted in the same set of theoretical works, that $Ge_{1-x}Sn_x$ must have higher carrier mobility's than other semiconductor compounds or alloys, with band gaps in the same energy range, due to the absence of polar phononic dispersion [6].

When the alloy is prepared starting from Ge, a direct gap material is eventually obtained, that evolves from indirect to direct electronic band gap as a result of the fact that the Γ-point conduction-band minimum decreases in energy value more rapidly than the L-point valleys at the [111] points at the border of the Brillouin Zone [10,11,14,15]. Moreover, as $Ge_{1-x}Sn_x$ alloys are always prepared as strained films grown mainly either on Si or Ge substrates, the presence of compressive strain is expected to decrease the Sn concentration at which the indirect $L_6 \rightarrow \Gamma_8$ to direct $L_7 \rightarrow \Gamma_8$ band-gap crossover is observed [7,12,15-18].

The growth of these $Ge_{1-x}Sn_x$ alloys, however, has been limited because it presents severe difficulties, that have to be overcome, stemming from to the following three factors: (a) limited Sn miscibility in the Ge (less than 1%) or of the Ge in Sn (less than 0.6%) [19]; (b) the tendency of the diamond tin phase (α-Sn) to spontaneously suffer a transition to the metallic phase (β-Sn) at temperatures higher than 13.2 °C [20]; (c) with increasing Sn composition, the high diffusivity of Sn into Ge and the free energy difference among the metastable state and the equilibrium state of the two phases causes a phase separation and promotes the transformation from the meta stable to the stable phase $\alpha \rightarrow \beta$ [20]. Low temperature deposition is then needed. An additional obstacle to overcome in the epitaxial growth of $Ge_{1-x}Sn_x$ on Ge, the preferred substrate, is that the lattice constant mismatch between α-Sn (a_{Sn} = 6.4892 Å) and Ge (a_{Ge} = 5.6579 Å) is 14.7% [21].

The difficulties to prepare $Ge_{1-x}Sn_x$ on either Ge or Sn or any other substrate, have resulted in a notorious scarcity of data in the literature for almost all of their physical properties, as well as the interest mentioned to use it as a column IV direct bandgap material in the far and medium infrared. We find this facts as a challenge for synthesize, study and determine as many of the physical properties of $Ge_{1-x}Sn_x$ as possible.

In this article, we present a study of $Ge_{1-x}Sn_x$ alloys of low Sn concentration $0.01 \leq x \leq 0.14$ samples grown on either Ge(001) or GaAs(001) by radio frequency sputtering [22]. GaAs substrates were chosen, in addition to Ge, because of the very similar lattice constants of GaAs and Ge (a_{GaAs} = 5.6535 Å).The samples with $0.01 \leq x < 0.06$ have a highly heterogeneous structural conformation, with a thin superficial layer of contrasting concentration. The study reveals that for higher Sn concentrations this phenomenon is not detected and the samples grow partially or totally relaxed with a high density of dislocations and a more homogenous Sn con-

centration and conformation for the bulk of the sample. The epitaxial thicknesses were estimated from measurements and simulations of High Resolution X Ray Diffraction (HRXRD) rocking curves, measured by a profilometer and in two samples by High Resolution Transmission Electron Microscopy (HRTEM) as described in the next section.

2. Experimental

The $Ge_{1-x}Sn_x$ alloys were grown in a R.F. Magnetron Sputtering on Ge(001) and GaAs(001) substrates. The base pressure in the growth chamber was better than 1×10^{-7} mbar and high purity Ar (99.999%) was used in the sputtering process. The targets, Ge(99.999%) and Sn(99.999%) were 10 cm in diameter with a 5 cm separation between target and samples in order to obtain good layer homogeneity. The targets were each biased by a rf power between 10-60 watts. The substrate preparation procedure previous to crystal growth was as following: Ge(001) wafers were previously polished and then ultrasonically degreased in successive rinses of trichloroethylene, acetone, and methanol for 10 minutes. After degreasing, the samples were ultrasonically rinsed in deionized water for 15 minutes and then blown dry in N_2. The samples were exposed in air to 33 mW/cm^{-2} of radiation from an UV lamp (line emission in 366 nm) during 30 minutes. This procedure is done in order to remove the native oxide layer (C contamination) and form a thin non-permeable and passive amorphous GeO_3 layer by an ultraviolet-ozone induced process. The GeO_3 layer is easily removed by desorption at temperatures $T_d \geq 390$ °C for periods $t_d \geq 30$ minutes. The procedure provides clean Ge surfaces with sharp Reflection High Energy Electron Diffraction (RHEED) patterns and no impurities detectable by Auger or X-Ray photoelectron spectroscopy as is reported in Ref. 23. GaAs wafers were cleaned in the same way as Ge wafers but without UV exposition.

In order to have a reliable measurement of the actual substrate temperature T_s, the substrates were attached to a molybdenum plate using small steel holders that maintain the substrate in good thermal contact. This procedure allows us to obtain reliable temperatures and reproducibility with variations smaller than ±5 °C. The substrate temperature was varied from 150 to 170 °C. The pressure in the chamber during the growth was kept between 2 and 5×10^{-2} mbar. A Ge buffer layer of similar thickness was grown for all samples ($\sim$17000 nm). Afterwards, on top of this Ge buffer layer, the $Ge_{1-x}Sn_x$ alloy is grown, typically a few thousand nanometers in thickness. A group of samples of these layers was obtained by varying the exposure time of the substrates under the Ge and Sn targets for total growth times from 3 to 30 minutes. The resultant thickness varied from 130 to 1240 nm as measured with a profilometer.

All samples were measured by HRXRD, using a Bartels monochromator in the Ge (022) reflection mode, with a Cu anode as the source of X-ray radiation. The X-ray source was operated at 30 kV and 30 mA. Diffraction profiles were obtained from the (004), (115), (-1-15) reflections. At each measurement, the sample was tilt adjusted to bring the sample diffraction vector into the diffractometer plane. The angular separation between substrate peak and layer peak reflections was determined by least squares fits to Gaussian profiles in all cases. We also used the powder X-ray diffraction technique to analyze the $Ge_{1-x}Sn_x$ layer grown on the pseudomorphical Ge buffer layer in order to corroborate our HRXRD results. The Sn content was established from the high resolution X-ray diffraction rocking curves, assuming a linear behavior of the bulk lattice parameter of the $Ge_{1-x}Sn_x$ alloy. In addition, and only for pseudomorphic layers ($x \leq 0.06$), the epitaxial thickness is determined from the width of the (004) reflection layer diffraction peak.

Raman scattering experiments were performed at room temperature using the 5145 Å line of an Ar laser at normal incidence for excitation. This geometry allows, based on Raman selection rules, the measurement of LO phonon scattering in both diamond and zincblende crystal structures. The light was focused to a diameter of 3 μm at the sample using a 100x (numerical aperture = 0.9) microscope objective. The laser power used in these measurements was 0.75 mW corresponding to a power density of 1.1×10^4 W$\cdot$ cm^{-2}. The estimated steady-state surface temperature increase, based on the heat transfer model developed by Lax for the case in which the source is a focused continuous-wave laser [24] was $\sim$3 – 5°C. In any case, care was exercised not to heat the sample to the point of changing its Raman spectrum.

Scattered light was analyzed using a Jobin-Yvon T64000 triple spectrometer, operating in the subtractive configuration, and a multichannel charge-coupled device detector cooled to 140 K. Absolute spectral feature position calibration to better than 0.5 cm^{-1} was performed using the observed position of the Ar laser plasma line 34 (5287.0 Å) which is red-shifted by 521.2 cm^{-1} from the excitation line.

3. Results

3.1. Structural studies from rocking curves

Figure 1 shows a typical rocking curve of $Ge_{1-x}Sn_x$/Ge pseudomorphic layers around the (004) reflection with $x = 0.02$. The separation between the diffraction peaks of the substrate and the $Ge_{1-x}Sn_x$ layers depends basically on two factors, i) strain produced in $Ge_{1-x}Sn_x$ layers by the substrate, and ii) Sn concentration in the alloys. However, in spite of the existence of these two contributions, in this case, the observed alloy diffraction peak shift is dominated mostly by the Sn concentration as has been mentioned elsewhere [22]. The peak associated to the $Ge_{1-x}Sn_x$ layer is fitted to a Gaussian curve in order to determine the Full Width at Half Maximum (FWHM) and then the layer thickness. This peak is not dislocation broadened because the layer is pseudomorphic to the Ge substrate.

It is experimentally found that only alloys with low Sn $\leq$ 5% concentration have pseudomorphic characteristics, since the in-plane lattice constant in $Ge_{1-x}Sn_x$ grown on Ge

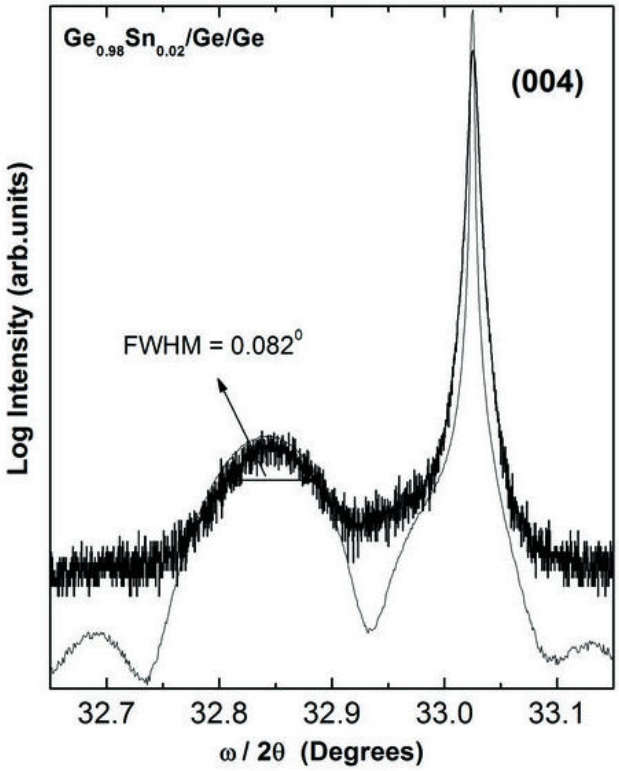

FIGURA 1. Rocking curve of a $Ge_{0.98}Sn_{0.02}$/Ge pseudomorphic layer in the (004) difraction plane.

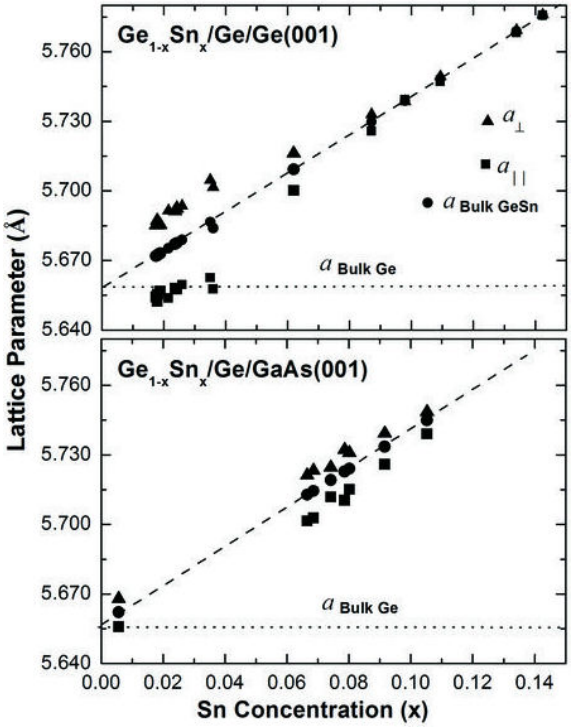

FIGURE 2. Lattice constants obtained from HRXRD analysis are shown. The dashed lines are used as visual helps to show the bulk lattice constant alloy behaviour. The lattice constants of Ge and GaAs, dotted lines in a) and b), respectively, are shown in order to compare them with the in-plane lattice parameters.

has the same value as the substrate lattice constant, within the experimental uncertainty as shown in Fig. 2. When the Sn concentration is increased, a partial process of relaxation is observed and in-plane and in-growth lattice parameters change continuously to the bulk lattice constants of the alloys. In more detail, in Fig. 2 the $a_\perp$ (in-growth) and $a_\parallel$ (in-plane) lattice constants are shown as function of Sn concentration. It is readily observed that for the alloys grown on Ge, when the concentration $x \sim 0.09$ is reached, the relaxation process is completed and essentially the in-plane lattice constants reach the bulk lattice constants of the alloy. In contrast, for the alloys grown on GaAs the relaxation process is not finished even for the sample with the highest Sn concentration.

This difference in behavior between the $Ge_{1-x}Sn_x$/Ge/Ge and the $Ge_{1-x}Sn_x$/Ge/GaAs alloys may be understood as due to the differences in the Linear Thermal Expansion Coefficients α (LTEC) between $Ge_{1-x}Sn_x$, Ge and GaAs. We estimate that the maximum strain due to this difference is around $\varepsilon_\parallel = 2 \times 10^{-6}$ for the sample $Ge_{1-x}Sn_x$/Ge/Ge(001) with $x = 0.14$. This is a small amount due to the LTEC of the $Ge_{1-x}Sn_x$ alloys and Ge have very close values. The LTEC is also a function of temperature, the LTEC of the alloy crosses that of Ge around 355 K (∼80 °C), hence both LTEC of the alloy and substrate, counterbalance to produce $\varepsilon_\parallel \approx 0$ ($\varepsilon = \int(\alpha_{\text{alloy}} - \alpha_{\text{substrate}})dT$) [11]. In the case of $Ge_{1-x}Sn_x$/Ge/GaAs(001), the strain due to LTEC differences between the alloy with $x = 0.14$ and GaAs substrate is expected to be $\varepsilon_\parallel = 1.5 \times 10^{-3}$, a value three orders of mag-

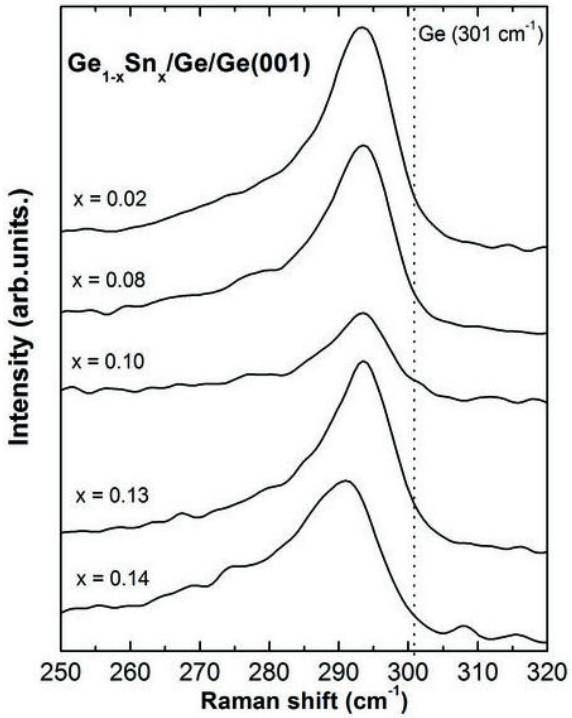

FIGURE 3. Raman spectra of rf-sputtered grown thin films of $Ge_{1-x}Sn_x$/Ge/Ge(100). The Sn concentration is established by HRXRD.

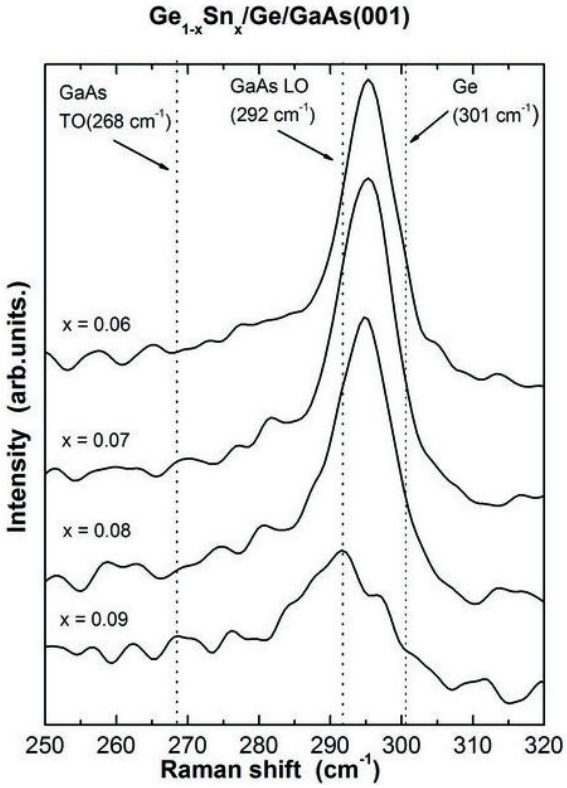

FIGURE 4. Raman spectra of rf-sputtered grown thin films of $Ge_{1-x}Sn_x$/Ge(100)/GaAs.

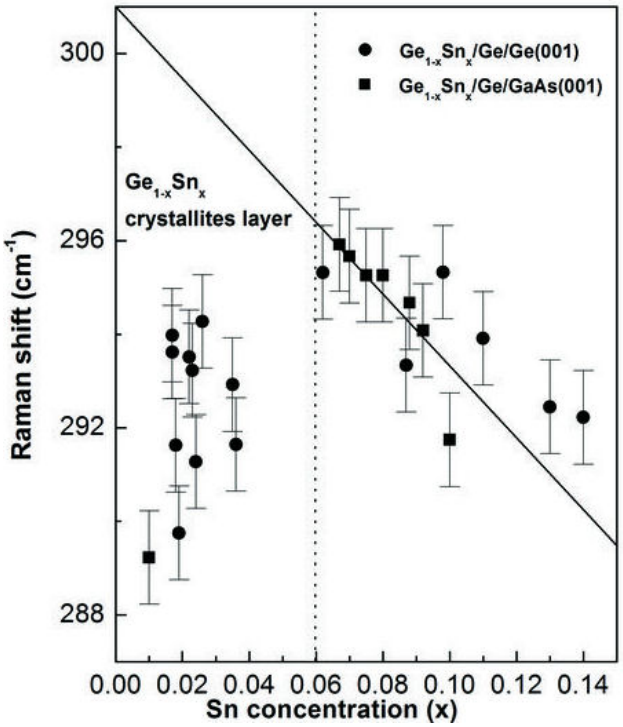

FIGURE 5. Summary of the peak positions of the Raman shifts of LO-Ge mode in $Ge_{1-x}Sn_x$ alloys grown on Ge(001 and GaAs(001).

nitude higher than in the case of Ge substrates. This strain produces a difference between $a_\perp$ and $a_\parallel$ that is consistent in magnitude with the data observed for all concentrations of Sn in Fig. 2.

Figures 3 and 4 show the Raman shift spectra of $Ge_{1-x}Sn_x$ alloys with different Sn concentration, grown on top of Ge (001) and GaAs(001) substrates, respectively. The Sn concentrations x indicated are determined by HRXRD. The alloy thicknesses are always larger than the laser penetration depth.

In these Figures the Longitudinal Optical mode (LO) Ge-Ge phonon line is observed. The LO-line shapes have the characteristics of $Ge_{1-x}Sn_x$ crystallites, a situation that contrast with better quality Molecular Beam Epitaxy (MBE) and Metal Organic Chemical Vapour Deposition (MOVCD) films [26,27]. The expected positions, for bulk unstressed samples, of the LO-Ge phonon, as well as the LO and Transverse Optical (TO) phonons of GaAs, are indicated with dotted lines. It is clear that the LO-Ge mode is asymmetric and shifted to lower energies as expected for $Ge_{1-x}Sn_x$ alloy. It is standard to characterize the total FWHM (Γ) of this asymmetric line in terms of two half widths (HW) $\Gamma_0 = \Gamma_A + \Gamma_B$, where Γ_A corresponds to the HW of the Raman line low energy side, as measured from the central frequency ω_0. Γ_A is visibly larger than the right or high energy side HW Γ_B.

The peak positions of the LO-Ge Raman mode are plotted in Fig. 5 for the whole set of sputtered grown $Ge_{1-x}Sn_x$ samples, on top of Ge or GaAs. The solid line indicates our

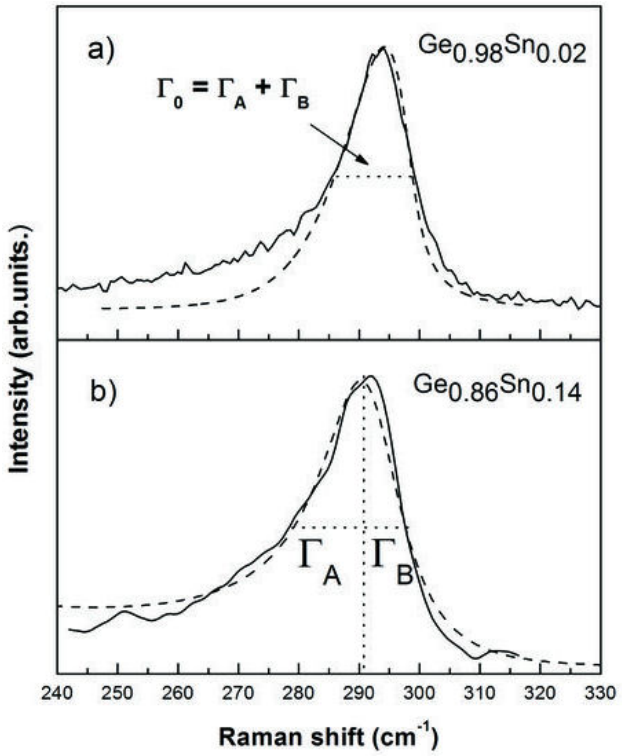

FIGURE 6. a) Spatial Correlation Model, weighted Lorentzian fit of the Raman LO-Ge mode in $Ge_{0.98}Sn_{0.02}$. b) Illustration of the asymmetry of the LO-Ge mode in $Ge_{1-x}Sn_x$ alloys.

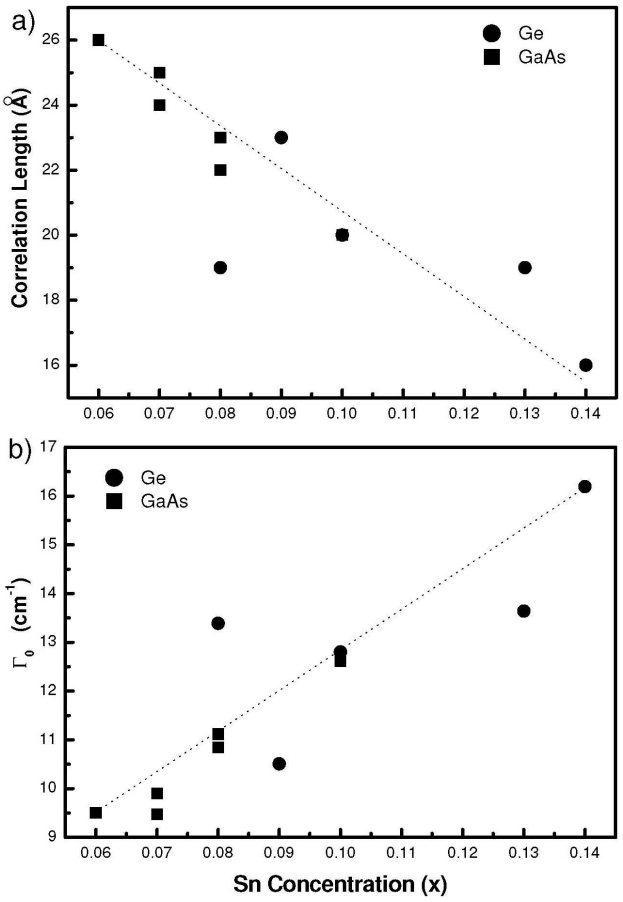

FIGURE 7. . a) Observed dependence of the phonon propagation correlation length, for films with Sn>0.06, grown on top of either Ge or GaAs. b) Similar result for the FWHM of the LO Raman lines for films with Sn>0.06, grown on top of either Ge or GaAs.

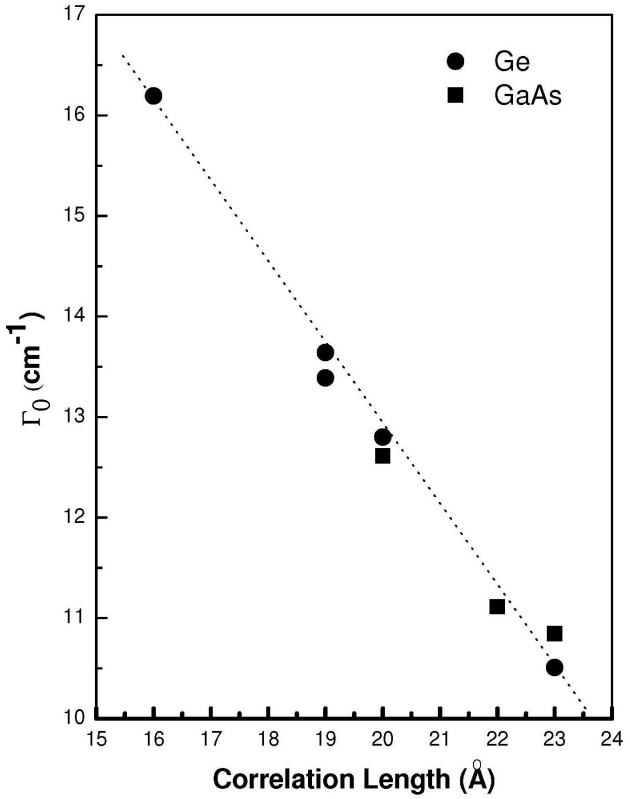

FIGURE 8. Phonon propagation correlation lengths vs. FWHM, LO Raman lines, in $Ge_{1-x}Sn_x$ films with Sn>0.06, grown on top of either Ge or GaAs.

predictions of the corresponding Raman shifts obtained from the empirical relationship $\Delta\omega_{\text{GeSn}} = 301.0\ \text{cm}^{-1} - 76.8x\ \text{cm}^{-1}$ obtained from MBE grown $Ge_{1-x}Sn_x$/Ge [25], which was essentially corroborated in a Raman report for similar material in Ref. 26, that may be expected to apply also for $Ge_{1-x}Sn_x$ samples grown on GaAs substrates, as this compound has almost identical lattice constant as Ge.

In this Fig. 5, it is observed immediately, that the partially relaxed films with Sn concentrations $x > 0.06$, according to the HRXRD of Fig. 2, show a Raman shift comparable to that predicted from the empirical relationship mentioned above. However, the films with lower concentration, which are pseudomorphic with the substrate exhibit a different unexpected response.

As discussed from the HRXRD results in Fig. 2, all samples with Sn $\leq$ 6% grown at low temperatures suffer a structural transition from epitaxial growth to a $Ge_{1-x}Sn_x$ crystallites growth regime. This transition was observed by means of a XRD study at both high and low resolutions [23]. This effect has also been observed in MBE grown Ge at low temperatures ($\sim 180\,^{\circ}$C) [27]. Due to the relatively shallow laser penetration depth (170 Å), the Raman shifts observed in these low Sn concentration sample must originate in the crystallite layers of $Ge_{1-x}Sn_x$ at their surfaces.

These layers of $Ge_{1-x}Sn_x$ crystallites at the surface form a "crust" or cap at, which the Raman response clearly indicates that is Sn enriched. The Sn concentration of the cap is higher with respect to the average Sn concentration of the pseudomorphic film, which is probed in its full depth by the HRXRD rocking curves. From the linear relation $\omega_{\text{GeSn}} = 301.0\ \text{cm}^{-1} - 76.8x\ \text{cm}^{-1}$ the observed.

Raman shifts for these crystallites samples of average "bulk" $x < 0.06$ should correspond to surface caps with Sn enriched concentration from 0.10 to 0.16, a result which is consistent with the strong tendency of the Sn to migrate to the surface of the alloys during the growth, a problem that affects the growth of the $Ge_{1-x}Sn_x$ alloys. No similar enriched cap was observed for the samples with more than 6% Sn concentration. This result has to be explained from the complex chemical process of the growth outside of thermodynamic equilibrium of these samples, which is not a simple theoretical task, and beyond the scope of the present report.

3.2. Study of the polycrystalline characteristics from the asymmetry of the Raman lines

The asymmetry of the Raman lines provides important information about the structural properties of a material. In the frame of the Spatial Correlation Model (SCM), and the fit

to the Γ_0, Γ_A and Γ_B, by means of a weighted Lorentzian curve, throughout the full phonon optical branch in the Brillouin Zone [28,29], the average spatial correlation length (L) may be established. This can be interpreted as the average size of the constitutive structures of nanometric dimensions of the material in which the phonon oscillations propagate. The SCM predicts that the asymmetric line may be calculated from:

$$I(\omega) \propto \int_0^1 \exp(-\frac{q^2L^2}{4}) \frac{dq}{(\omega - \omega(q))^2 + \left(\frac{\Gamma_0}{2}\right)^2} \qquad (1)$$

The integral is performed in the reciprocal space, approximating the actual Brillouin zone of the zinc blende material by a sphere, where L is now the diameter of the correlation region in the direct space, a is the lattice constant, q is the phonon wavevector $2\pi/a$, Γ_0 is the intrinsic Lorentzian phonon width of the non perturbed bulk sample, and $\omega(q)$ is the phonon dispersion curve, given for the Lo branch in Ge as:

$$\omega(q) = 271.5 \ \text{cm}^{-1} + 29.5\cos(\pi q) \ \text{cm}^{-1} \qquad (2)$$

In the calculations, the Ge parameters were used, as the phonon branches of $Ge_{1-x}Sn_x$ are unknown, justified by the fact that as our samples have $x < 0.14$, the Ge is the predominant element in the alloy matrix. Figure 6 shows the fitting of the model to the Raman shift of the LO-Ge mode of two samples: a) $Ge_{0.98}Sn_{0.02}$ and b) $Ge_{0.86}Sn_{0.14}$. There is clearly a good fit between the experimental Raman and the model for samples with or without the top $Ge_{1-x}Sn_x$ crystallite layer and thus the obtained phonon frequencies are reliable in both cases.The fitting reproduces the FWHM and the asymmetrical shape by just varying the diameter of the correlation region L.

The experimentally obtained behavior between the average correlation length L and the Sn concentrations in the alloys with $x > 0.06$ grown on both Ge or GaAs substrates is shown in Fig. 7a. The similar relation obtained for the width $\Gamma_0 = \Gamma_A + \Gamma_B$ is shown in Fig. 7b. The observed relation between the Raman FWHM and the correlation length of these $Ge_{1-x}Sn_x$ alloys is shown in Fig. 8. In these three plots, almost linear correlations are observed in practically all cases for both sets of samples grown in either Ge or GaAs.

These linear correlations among L, Γ_0 and the Sn concentrations, are indicative that when the percentage of Sn increases in the alloy, the average size of the crystallite where the Ge-LO phonons propagate decreases, *i.e.* the amount of defects increases in the film, something that may be expected because the overall monotonically increasing lattice misfit, the compositional disorder introduced by the Sn replacing the predominant Ge-matrix (alloy effect) as well as the fact that in rf-sputtering, the intense atomic bombardment during the growth should result in the formation of many local defects. This set of physical effects, should cause the increment in FWHM Γ_0 and the asymmetry of the Raman LO-Ge line.

4. Conclusions

The Raman results of sputtered growth $Ge_{1-x}Sn_x$ alloys thin films indicate that the samples with a bulk $x < 0.06$ Sn concentration, are covered with an enriched Sn alloy that covers the topmost layer, at least 170 Å in thickness. The Raman results indicate that for samples with a bulk $x > 0.06$ no similar enhancement in the Sn concentration at the surface exists. For these samples there are linear correlations among L, Γ_0 and the Sn concentrations, indicative that when Sn percentage increases in the alloy, the average size of the crystalline coherence region where the Ge-LO phonons propagate, decreases. Essentially the same correlations are observed for $Ge_{1-x}Sn_x$ alloys grown either Ge or GaAs substrates. The different residual strain in the layers may be understood as due to the differences in the linear thermal expansion coefficients of Ge and GaAs. This result should originate from the intense atomic bombardment produced during the sputtering growth, additional to the disorder produced by the Sn alloying. These facts may limit the formation of crystalline material for a Sn concentration where this correlation length tends to zero, for the rf-sputtering grown material.

Acknowledgments

The authors acknowledge the financial support from Consejo Nacional de Ciencia y Tecnología (CONACyT) México, through grants CB-2009-01 133428, 152155 and 78943; from FRC-UASLP, and the access to the Laboratorio Nacional de Análisis Físicos, Químicos y Biológicos-UASLP, during the course of this research.

1. Kouvetakis and J. Menéndez, *Appl. Phys. Lett.* **98** (2011) 061109.
2. J. Mathews, R. Roucka, J. Xie, S. Q. Yu, J. Menéndez and J. Kouvetakis, *Appl. Phys. Lett.* **95** (2009) 133506.
3. S. Su *et al*., *Opt. Express* **19** (2011) 6400.
4. G. Sun, R. A. Soref, and H. H. Cheng, *J. Appl. Phys.* **108** (2010) 033107.
5. G. Sun, R. A. Soref, and H. H. Cheng, *Opt. Express* **18** (2010) 19957.
6. C. H. L. Goodman, *IEEE Proc.* **129** (1982) 189.
7. M. Bauer *et al*., *Appl. Phys. Lett.* **81** (2002) 2992.
8. Y. Y. Fang, J. Tolle, R. Roucka, A. V .G. Chizmeshya, J. Kouvetakis, V. R. D'Costa and J. Menéndez, *Appl. Phys. Lett*. **90** (2007) 061915.

9. Junqui Xie, J. Tolle, V. R. D'Costa, A. V .G. Chizmeshya, J. Menéndez and J. Kouvetakis, *Appl. Phys. Lett*. **95** (2009) 181909.
10. D. W. Jenkins and J. D. Dow, *Phys. Rev. B* **36** (1987) 7994.
11. K. A. Mader, A. Baldereschi and H. Von Kanel, *Solid State Commun.* **89** (1989) 1123.
12. R. A. Soref and L. Friedman, *Superlattices Microstruct.* **14** (1993) 189.
13. S. Groves and W. Paul, *Phys. Rev. Lett.* **11** (1963) 194.
14. S. Oguz, W. Paul, T. F. Deutch, B. Y. Tsaur and D. V. Murphy, *Appl. Phys. Lett.* **43** (1983) 50.
15. Gang He and Harry A. Atwater, *Phys. Rev. Lett.* **79** (1997) 1937.
16. R. Ragan and H. A. Atwater, *Appl. Phys. Lett.* **77** (2000) 3418.
17. H. Pérez Ladrón de Guevara, A. G. Rodríguez, H. Navarro-Contreras, and M. A. Vidal, *Appl. Phys. Lett.* **84** (2004) 4532.
18. H. Pérez Ladrón de Guevara, A. G. Rodríguez, H. Navarro-Contreras, and M. A. Vidal, *Appl. Phys. Lett*. **91** (2007) 161909.
19. Bull, *Alloy Phase Diagrams* **5** (1984) 266.
20. G. A. Busch and A. Kern, in *Solid State Physics*, **Vol. 11** (Academic, New York, 1961), pp. 1-40.
21. Landolt-Bornstein, *Numerical data and functional relationships in science and technology*, New series III, **Vol. 17a** (Springer-Verlag, Berlin, 1982).
22. H. Pérez Ladrón de Guevara, A. G. Rodríguez, H. Navarro-Contreras, and M. A. Vidal, *Appl. Phys. Lett.* **83** (2003) 4942.
23. H. Pérez Ladrón de Guevara, "Crecimiento y caracterización de aleaciones $Ge_{1-x}Sn_x$", PH. D. Thesis UASLP, (2004).
24. M. Lax, *J. Appl. Phys.* **48** (1977) 3919.
25. M. Rojas-López, H. Navarro-Contreras, P. Desjardins, O. Gurdal, J. Karlsson and J. E. Greene. *J. Appl. Phys.* **84** (1998) 2219.
26. Hai Lin, Robert Chen, Yijie Huo, Theodore I. Kamins, and James S. Harris, *Appl. Phys. Lett.* **98** (2011) 261917.
27. K. A. Bratland, Y. L. Foo, J. A. N. T. Soares, T. Spila, P. Desjardins, and J. E. Greene, *Phys. Rev. B* **67** (2003) 125322.
28. K. K. Tiong, P. M. Amirtharaj, F. H. Pollak and D. E. Aspnes, *Appl. Phys. Lett.* **44** (1984) 122.
29. P. Parayantal and F. Pollak, *Phys. Rev. Lett.* **52** (1984) 1822.